

# Influence of Asymmetric Factors on Outlet Wedge Shape of Hot Rolled Pure Titanium Medium and Thick Plate

Yu Hui<sup>1,2</sup>, Li Wei<sup>1</sup>, Huang Zhaomeng<sup>1</sup>, Wang Sanzhong<sup>1</sup>, Liu Ligang<sup>1</sup>

<sup>1</sup> College of Mechanical Engineering, Yanshan University, Qinhuangdao 066004, China; <sup>2</sup> National Engineering Research Center for Equipment and Technology of Cold Steel Rolling, Yanshan University, Qinhuangdao 066004, China

**Abstract:** Aiming at the possible wedge shape problem of rolling section in the hot rolling process of pure titanium medium and thick plate, combined with the asymmetric characteristics of four-high rolling mill equipment and technology, the elastic deformation model of double cantilever beam roll system was established based on the influence function method. The influence of asymmetrical factors such as the centring error, stiffness difference of mill stand, wedge shape of billet, transverse temperature difference of workpiece and other asymmetric deformation parameters on rolling section wedge shape was investigated. The results indicate that the effect of the above influence factors increases with the increase of the plate width and rolling reduction. The influence of the inlet wedge shape on the outlet wedge shape increases with the increase of the plate width and the decrease of the rolling reduction.

**Key words:** influence function method; pure titanium; hot rolling; medium and thick plate; wedge prediction

During hot rolling process of pure titanium medium and thick plate, the asymmetric deformation in the width direction of the rolling piece will cause the heterogeneous distribution of the thickness on both sides of the rolled piece, and lead to poor wedge shape of the section. Serious wedge shape of the section will result in side bending and off tracking of the rolled piece, which affect the stability of the rolling process and the quality of the final product<sup>[1-3]</sup>. The production practice and previous research indicate that the asymmetrical factors such as centring error of rolling, inlet wedge of workpiece, stiffness difference of mill stand on both sides, transverse temperature difference of the workpiece will significantly influence the wedge shape of medium and thick plate<sup>[4-8]</sup>. The wedge shape is usually controlled by adjusting the roll inclination in the production site, and it is difficult to control the influencing factors of wedge shape effectively, and finally it is difficult to achieve the thickness precision of the pure titanium plate in the hot

rolling to meet the process requirements.

The influence function method is one of the calculation methods of plate shape and plate thickness in plate and strip rolling process. It is widely used in plate thickness calculation, plate shape calculation, rolling force calculation, roll system stress analysis, etc<sup>[9-12]</sup>. In previous literatures, it is assumed that the frame and roll system of a four-high mill are arranged symmetrically, and the upper and lower rollers have the same roll shape and the center line of rolling and roll overlaps<sup>[13-15]</sup>. However, the actual field tracking shows that the calculation conditions of the above assumptions are often not satisfied, sometimes far away from each other due to the problems of machining errors, installation errors and field working conditions of rolling mill components.

Therefore, because of asymmetrical rolling force distribution caused by asymmetric factors during hot rolling process of pure titanium medium and thick plate, the uneven of plate thickness and rolling section wedge shape

Received date: July 26, 2019

Foundation item: Special Funds for the Development of Civil-Military Integration Industry in Hebei Province; Natural Science Foundation of Hebei Province of China (E2016203217)

Corresponding author: Yu Hui, Ph. D., Professor, College of Mechanical Engineering, Yanshan University, Qinhuangdao 066004, P. R. China, E-mail: yu-hui@ysu.edu.cn

Copyright © 2020, Northwest Institute for Nonferrous Metal Research. Published by Science Press. All rights reserved.

appears. The combination of the asymmetric characteristics of four-high rolling mill equipment and process on the basis of field test and theoretical research was investigated. In order to study the influence of asymmetric factors on the wedge shape of rolling section and to provide a basis for the wedge shape control on site, the elastic deformation model of double-cantilever beam roll system was established based on the influence function method and coupled with the asymmetric calculation model.

## 1 Roll System Deformation Model Based on Influence Function Method

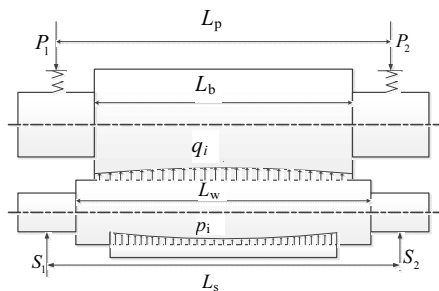
### 1.1 Roll system mechanical model

The pure titanium medium and thick plate was usually rolled by a four-high hot rolling mill. The asymmetric factors caused the asymmetrical rolling force distribution and the difference of the bounce on the two sides of the mill frame during rolling process<sup>[16-18]</sup>. Thus, the calculation model of roll system deformation of double cantilever beam was established. The force diagram of roll system is shown in Fig.1. It is assumed that the symmetric center of the roll is the fulcrum, and both sides of the fulcrum are connected with a cantilever beam. The roll system and the workpiece are divided into  $2n+1$  units (one unit at the centre of symmetry, the left and right sides of each  $n$  unit) with the reference of the backup roll. Number them from left to right, the length of each unit is  $\Delta x$ .

$$\Delta x = \frac{L_b}{2n+1} \quad (1)$$

It is assumed that the axial direction of the roll is in the  $x$  direction, and the zero point is set on the axial symmetric surface of the roll. Thus, the position coordinate corresponding to the  $i$  unit is  $x_i$ .

$$x_i = [i - (n+1)]\Delta x = [i - (n+1)]\frac{L_b}{2n+1} \quad (2)$$



$P_1, P_2$ -left and right supporting forces;  $L_w$ -length of work roll;  $p_i$ -rolling force distribution;  $L_s$ -distance between the fulcrums of bending roll cylinder;  $q_i$ -contact force distribution between roll;  $L_p$ -distance between pressure screws;  $S_1, S_2$ -left and right bending force;  $L_b$ -length of backup roll

Fig.1 Diagram of roller system force

The force and deformation between the work roll, backup roll and workpiece are discretized, and the concentrated force on the discrete element represents the distributed load on the element. The distribution of rolling force  $p_i$ , pressure between rolls  $q_i$  and outlet thickness  $h_i$  are obtained:

$$\vec{P} = [p_1, p_2, \dots, p_{2n+1}] \quad (3)$$

$$\vec{Q} = [q_1, q_2, \dots, q_{2n+1}] \quad (4)$$

$$\vec{h} = [h_1, h_2, \dots, h_{2n+1}] \quad (5)$$

### 1.2 Basic equation of influence function

According to previous literatures<sup>[19,20]</sup>, the roll system mechanical model is still established even if there are asymmetric factors during hot rolling process of pure titanium. The parameters of work roll bending influence function  $G_{ij}^w$ , backup roll bending influence function  $G_{ij}^b$ , work roll bending force influence function  $G_i^{sl}$  (left) and  $G_i^{sr}$  (right), backup roll support force influence function  $G_i^{pl}$  (left) and  $G_i^{pr}$  (right), backup roll and work roll flattening coefficient  $K_i$ , work roll and workpiece flattening coefficient  $K_i'$  can be derived. It is also used to calculate the subsequent coupled asymmetric model. Detailed equation is browsed in follows.

#### 1.2.1 Roll bending influence function under distributed load

The deflection influence function of work roll in section  $i$  induced by section  $j$  load, (section  $j$  load is rolling force or the pressure between rolls) in the left half roll system of the working roll ( $x_i \leq 0$ )  $G_{ij}^w$  is shown in Eq.(6):

$$\begin{cases} G_{ij}^w = k_w \left[ \left( \frac{-2x_i}{L_w} \right)^2 \left( 3 \left( \frac{-2x_j}{L_w} \right) - \frac{-2x_j}{L_w} \right) + (1+\nu_w) \frac{3k}{4} \left( \frac{-2x_i}{L_w} \right) \left( \frac{2D_w}{L_w} \right)^2 \right] (j \leq i) \\ G_{ij}^w = k_w \left[ \left( \frac{-2x_i}{L_w} \right)^2 \left( 3 \left( \frac{-2x_j}{L_w} \right) - \frac{-2x_j}{L_w} \right) + (1+\nu_w) \frac{3k}{4} \left( \frac{-2x_i}{L_w} \right) \left( \frac{2D_w}{L_w} \right)^2 \right] (j \geq i) \end{cases} \quad (6)$$

where  $i=1, 2, \dots, n; j=1, 2, \dots, n$ ;  $k_w$  is a constant coefficient,  $k_w = L_w^3 / 48E_w I_w$ ;  $E_w$  is the elastic modulus of work roll material (MPa);  $\nu_w$  is the Poisson's ratio of work roll material;  $I_w$  is the moment of inertia of the neutral axis of work roll cross section,  $I_w = \pi D_w^4 / 64$ ;  $D_w$  is the work roll diameter (mm);  $k$  is shear factor,  $k = 10/9$ .

The deflection influence function of work roll in section  $i$  induced by section  $j$  load (section  $j$  load is rolling force or the pressure between rolls) in the right half roll system of the working roll ( $x_i \geq 0$ )  $G_{ij}^w$  is shown in Eq.(7):

$$\begin{cases} G_{ij}^w = k_w \left[ \left( \frac{2x_i}{L_w} \right)^2 \left( 3 \left( \frac{2x_j}{L_w} \right) - \frac{2x_j}{L_w} \right) + (1+\nu_w) \frac{3k_w}{4} \left( \frac{2x_i}{L_w} \right) \left( \frac{2D_w}{L_w} \right)^2 \right] (j \leq i) \\ G_{ij}^w = k_w \left[ \left( \frac{2x_i}{L_w} \right)^2 \left( 3 \left( \frac{2x_j}{L_w} \right) - \frac{2x_j}{L_w} \right) + (1+\nu_w) \frac{3k_w}{4} \left( \frac{2x_i}{L_w} \right) \left( \frac{2D_w}{L_w} \right)^2 \right] (j \geq i) \end{cases} \quad (7)$$

where  $i=n+2, n+3, \dots, 2n+1; j=n+2, n+3, \dots, 2n+1$ .

The elastic bending influence function  $G_{ij}^b$  of the backup roll is the same as that of the work roll. Whereas,  $E_w, I_w, \nu_w$  and  $D_w$  of the workroll in Eq.(6) and Eq.(7) are replaced

by  $E_b$ ,  $I_b$ ,  $v_b$  and  $D_b$  of the backup roll.

The elastic bending influence function of the left half roll system of the backup roll  $G_{ij}^b$  is shown in Eq.(8):

$$\begin{cases} G_{ij}^b = k_b \left[ \left( \frac{-2x_i}{L_b} \right)^2 \left( 3 \left( \frac{-2x_i}{L_b} \right) - \frac{-2x_i}{L_b} \right) + (1+v_b) \frac{3k_b}{4} \left( \frac{-2x_i}{L_b} \right) \left( \frac{2D_b}{L_b} \right)^2 \right] (j \leq i) \\ G_{ij}^b = k_b \left[ \left( \frac{-2x_j}{L_b} \right)^2 \left( 3 \left( \frac{-2x_j}{L_b} \right) - \frac{-2x_j}{L_b} \right) + (1+v_b) \frac{3k_b}{4} \left( \frac{-2x_j}{L_b} \right) \left( \frac{2D_b}{L_b} \right)^2 \right] (j \geq i) \end{cases} \quad (8)$$

The elastic bending influence function of the right half roll system of the backup roll  $G_{ij}^b$  is shown in Eq.(9):

$$\begin{cases} G_{ij}^b = k_b \left[ \left( \frac{2x_j}{L_b} \right)^2 \left( 3 \left( \frac{2x_j}{L_b} \right) - \frac{2x_j}{L_b} \right) + (1+v_b) \frac{3k_b}{4} \left( \frac{2x_j}{L_b} \right) \left( \frac{2D_b}{L_b} \right)^2 \right] (j \leq i) \\ G_{ij}^b = k_b \left[ \left( \frac{2x_i}{L_b} \right)^2 \left( 3 \left( \frac{2x_i}{L_b} \right) - \frac{2x_i}{L_b} \right) + (1+v_b) \frac{3k_b}{4} \left( \frac{2x_i}{L_b} \right) \left( \frac{2D_b}{L_b} \right)^2 \right] (j \geq i) \end{cases} \quad (9)$$

### 1.2.2 Roll bending influence function under concentrated force

The deflection influence function  $G_i^{sl}$  of the left roll bending force  $S_1$  of the work roll in section  $i$  is shown in Eq.(10):

$$G_i^{sl} = k_w \left[ \left( \frac{-2x_i}{L_w} \right)^2 \left( 3 \left( \frac{2l_{s1}}{L_w} \right) - \frac{-2x_i}{L_w} \right) + (1+v_w) \frac{3k_w}{4} \left( \frac{-2x_i}{L_w} \right) \left( \frac{2D_w}{L_w} \right)^2 \right] \quad (10)$$

where  $i=1, 2, \dots, n$ ;  $l_{s1}$  is the distance between the left roll bending force and roll system symmetry surface (mm),  $l_{s1} = L_s / 2$ .

The deflection influence function  $G_i^{sr}$  of the right roll bending force  $S_2$  of the work roll in section  $i$  is shown in Eq.(11):

$$G_i^{sr} = k_w \left[ \left( \frac{2x_i}{L_w} \right)^2 \left( 3 \left( \frac{2l_{s2}}{L_w} \right) - \frac{2x_i}{L_w} \right) + (1+v_w) \frac{3k_w}{4} \left( \frac{2x_i}{L_w} \right) \left( \frac{2D_w}{L_w} \right)^2 \right] \quad (11)$$

where  $i=n+2, n+3, \dots, 2n+1$ ;  $l_{s2}$  is the distance between the right roll bending force and roll system symmetry surface (mm),  $l_{s2} = L_s / 2$ .

The deflection influence function ( $G_i^{pl}$ ) of the left supporting force ( $P$ ) of the backup roll in section  $i$  is shown in Eq.(12):

$$G_i^{pl} = k_b \left[ \left( \frac{-2x_i}{L_b} \right)^2 \left( 3 \left( \frac{2l_{p1}}{L_b} \right) - \frac{-2x_i}{L_b} \right) + (1+v_b) \frac{3k_b}{4} \left( \frac{-2x_i}{L_b} \right) \left( \frac{2D_b}{L_b} \right)^2 \right] \quad (12)$$

where  $i=1, 2, \dots, n$ ;  $k_b$  is a constant coefficient,  $k_b = L_b^3 / 48E_bI_b$ ;  $l_{p1}$  is the distance between the left supporting force and the roll system symmetry surface (mm),  $l_{p1} = L_p / 2$ ;  $I_b$  is the moment of inertia of the neutral axis of the backup roll cross section,  $I_b = \pi D_b^4 / 64$ .

The deflection influence function ( $G_i^{pr}$ ) of the right supporting force ( $P_2$ ) of the backup roll in section  $i$  is shown in Eq.(13):

$$G_i^{pr} = k_b \left[ \left( \frac{2x_i}{L_b} \right)^2 \left( 3 \left( \frac{2l_{p2}}{L_b} \right) - \frac{2x_i}{L_b} \right) + (1+v_b) \frac{3k_b}{4} \left( \frac{2x_i}{L_b} \right) \left( \frac{2D_b}{L_b} \right)^2 \right] \quad (13)$$

where  $i=n+2, n+3, \dots, 2n+1$ ,  $l_{p2}$  is the distance between the right supporting force and the roll system symmetry surface (mm),  $l_{p2} = L_p / 2$ .

### 1.2.3 Elastic flattening coefficient equation

The elastic flattening coefficient  $K_i$  between the backup roll in section  $i$  and the work roll is shown in Eq.(14):

$$K_i = 2 \left[ \frac{1-v_w^2}{\pi E_w} \left( \ln \frac{2R_w}{b_i} + 0.407 \right) + \frac{1-v_b^2}{\pi E_b} \left( \ln \frac{2R_b}{b_i} + 0.036 \right) \right] \quad (14)$$

where  $b_i$  is the contact flattening half width between the work roll in section  $i$  and corresponding backup roll (mm);  $R_w$  and  $R_b$  are the work roll radius and backup roll radius (mm), respectively.  $b_i$  can be calculated by the Hertz formula, as shown in Eq.(15):

$$b_i = \sqrt{\frac{4q_i}{\pi \Delta x} \left( \frac{1-v_w^2}{E_w} + \frac{1-v_b^2}{E_b} \right) \frac{R_b R_w}{R_b + R_w}} \quad (15)$$

The flattening coefficient  $K'_i$  between the work roll in section  $i$  and the workpiece is shown in Eq.(16):

$$K'_i = \theta \left[ \ln \frac{4R_w}{\Delta h_i + 16\theta \frac{P_i}{\Delta x}} + \frac{32\theta \frac{P_i}{\Delta x}}{\Delta h_i + 16\theta \frac{P_i}{\Delta x}} \right] \quad (16)$$

where  $\theta$  is a constant coefficient.

## 1.3 Asymmetric computing model

### 1.3.1 Mill stand stiffness difference model

The stiffness difference on both sides of the mill stand inevitably leads to rigid tilting of the roll system. The backup roll rigid tilting displacement  $\Delta h_a$  and work roll tilting angle  $\beta$  are used to characterize roll system tilting. The functional relationship of the left mill stand stiffness  $k_l$ , right mill stand stiffness  $k_r$  and  $\Delta h_a$  is established by the mill stand spring Eq.(17):

$$\Delta h_a = \frac{P_2}{k_r} - \frac{P_1}{k_l} \quad (17)$$

where  $P_1$  and  $P_2$  are the left and right supporting force (N) of the backup roll, respectively.

### 1.3.2 Transverse temperature difference model of work-piece

The transverse temperature difference through a transverse temperature distribution  $T_i$  is introduced into the implementation. The vector is introduced into the influence function model by a deformation resistance model. The model of deformation resistance is shown in Eq.(18)<sup>[20]</sup>:

$$\sigma_i = (119 + 2197.5\varepsilon^{0.925} - 2145.6\varepsilon) \times (1 + 0.063 \ln \dot{\varepsilon}) [1 - 2.365(T_i)^{0.99}] \quad (18)$$

where  $\sigma_i$  is the deformation resistance of unit  $i$  of the workpiece;  $T_i$  is the thermodynamic temperature (K) of

the corresponding workpiece unit;  $\dot{\varepsilon}$  is the deformation velocity ( $s^{-1}$ ) and  $\varepsilon$  is the true strain.

1.3.3 Billet wedge shape model

The wedge shape of billet is introduced through the thickness distribution  $H_i$  of the plate entrance and is brought into the model by the rolling force function. Rolling force is shown in Eq.(19):

$$p_i = 1.15\sigma_i\sqrt{R_w(H_i - h_i)}BQ_p \quad (19)$$

where  $i=1, 2, \dots, 2n+1$ ;  $p_i$  is the rolling force of the workpiece unit  $i$  (N);  $B$  is the average width of the workpiece before and after rolling pass (mm);  $Q_p$  is the influence coefficient of the stress state;  $H_i$  is the plate entrance thickness distribution (mm);  $h_i$  is the plate outlet thickness distribution (mm).

1.3.4 Billet centring error treatment

In the process of roll system discretization, the work roll, backup roll and the workpiece were all discretized with the same unit length, unit number and number of discrete units, as shown in Fig.2. The actual length of the workpiece is generally less than the length of the backup roll. Therefore, the actual corresponding unit of rolling element is defined as a real unit, and the unit beyond rolling element is defined as a virtual unit, while defining the type of workpiece units. When calculating the equation of influence function matrix, the corresponding equation of virtual units will be deleted. The corresponding unit number of the virtual and real rolling part should be adjusted according to the actual alignment error, which exists in the bite of the rolling part.

1.4 Deformation coordination and equilibrium equations of the coupled asymmetric calculation model

1.4.1 Deformation coordination equation between rolls

The deformation coordination equation between the work roll and backup roll on the left side of the fulcrum is shown in Eq.(20):

$$\frac{\Delta h_a}{L_p}x_i - \frac{\Delta D_i^b + \Delta D_i^w}{2} = \sum_{j=1}^n G_{ij}^w(q_j - p_j) - G_i^{sl}S_1 + \beta x_i + \sum_{j=1}^n G_{ij}^b q_j - G_i^{pl}P_1 - K(q_{n+1} - q_i) \quad (20)$$

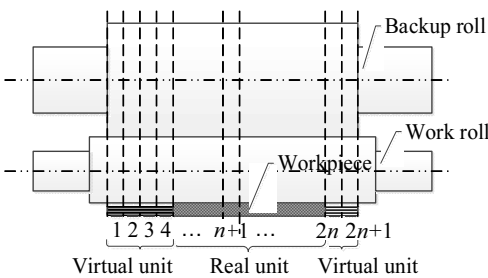


Fig.2 Numbered discrete element of workpiece

where  $i=1, 2, \dots, n$ ;  $\Delta D_i^b$  and  $\Delta D_i^w$  are corresponding roll crown of section  $i$  unit of the backup roll and work roll (mm), respectively.

The deformation compatibility equation between the work roll and backup roll on the right side is shown in Eq.(21):

$$\frac{\Delta h_a}{L_p}x_i - \frac{\Delta D_i^b + \Delta D_i^w}{2} = \sum_{j=n+2}^{2n+1} G_{ij}^w(q_j - p_j) - G_i^{st}S_2 + \beta x_i + \sum_{j=n+2}^{2n+1} G_{ij}^b q_j - G_i^{pr}P_2 - K(q_{n+1} - q_i) \quad (21)$$

where  $i=n+2, n+3, \dots, 2n+1$ .

1.4.2 Deformation coordination equation between work roll and workpiece

The deformation coordination equation between the workpiece and work roll on the left side of the fulcrum is shown in Eq.(22):

$$h_o - h_i = \sum_{j=1}^n G_{ij}^w(q_j - p_j) - G_i^{sl}S_1 + \beta x_i + K'(p_{n+1} - p_i) - \frac{\Delta D_i^w}{2} \quad (22)$$

where  $i=1, 2, \dots, n$ ;  $h_o$  is the outlet thickness of the centre (mm);  $h_i$  is the outlet thickness distribution of the workpiece (mm).

The deformation compatibility equation between the workpiece and work roll on the right side of the fulcrum is shown in Eq.(23):

$$h_o - h_i = \sum_{j=n+2}^{2n+1} G_{ij}^w(q_j - p_j) - G_i^{st}S_2 + \beta x_i + K'(p_{n+1} - p_i) - \frac{\Delta D_i^w}{2} \quad (23)$$

where  $i=n+2, n+3, \dots, 2n+1$ .

1.4.3 Force balance equation

The force and moment balance equation of the work roll is shown in Eq.(24) and Eq.(25):

$$\sum_{i=1}^{2n+1} q_i = \sum_{i=1}^{2n+1} p_i + S_1 + S_2 \quad (24)$$

$$\sum_{i=1}^{2n+1} q_i x(i) + S_1 \frac{L_s}{2} = \sum_{i=1}^{2n+1} p_i x(i) + S_2 \frac{L_s}{2} \quad (25)$$

The force and moment balance equation of the backup roll is shown in Eq.(26) and Eq.(27):

$$P_1 + P_2 = \sum_{i=1}^{2n+1} q_i \quad (26)$$

$$\sum_{i=1}^{2n+1} q_i x(i) + P_1 \frac{L_p}{2} = P_2 \frac{L_p}{2} \quad (27)$$

In summary, a total of  $6n+6$  equations are established. The outlet thickness of the centre  $h_o$  is known as a given constraint during calculation. Thus, the pressure between rolls  $q_i$ , rolling force  $p_i$ , outlet thickness distribution of the workpiece  $h_i$ , rigid tilting displacement of backup roll  $\Delta h_a$  and tilting angle of working roll  $\beta$  can be obtained.

1.5 Calculation flow

The flow chart of computation is shown in Fig.3. The contact pressure distribution between rolls and the outlet thickness distribution of the workpiece are revised by the exponential smoothing method. During program calculation,

the outlet thickness distribution was first assumed, and simultaneous deformation coordination and balance equations were performed, and the rolling force distribution and pressure distribution between rollers were iteratively solved. Then, according to the rolling force equation, the calculated rolling force distribution was reversely calculated based on the outlet thickness distribution, and then the assumed outlet thickness distribution was revised. Repeat iterating until all parameters meet the set convergence accuracy.

## 2 Influence of Asymmetric Factors on Wedge Shape of Section

The medium and thick plate of pure titanium (Table 1 shows chemical component of pure titanium billets) rolled by 4300 mm hot rolling unit (see Table 2 for equipment parameters) is taken as the research object in order to investigate the influence of asymmetrical factors on the outlet section wedge shape of hot rolled pure titanium medium and thick plate. The specifications are as follows: the billet thickness is 139 mm, the width is 1433 mm, the length is 3595 mm, the finished product thickness is 24 mm, the width is 1455 mm and the length is 20 497 mm. The rolling process parameters are shown in Table 3. The effects of asymmetrical factors of the inlet wedge shape of workpiece, the centring error of workpiece, the stiffness difference on both sides of the mill stand and the transverse temperature difference of workpiece on the outlet section wedge shape of workpiece were analyzed. In order to analyze the influence of a single factor on the outlet section wedge shape, other factors are assumed to remain unchanged.

### 2.1 Model validation

Fig.4 shows the average rolling force of pure titanium plate of the specification after 6 passes of rolling, and the comparison between the average rolling force of each pass and the calculated value of the model shows that they are in good agreement with each other, and the relative error is within  $\pm 8\%$ . Ultrasonic thickness measuring instrument was used to measure the thickness of the final titanium plate along the width direction after rolling. 11 points of the remaining middle part after removing 50 mm from each side of the width were averagely measured. A total of 3 groups of thickness values were measured to obtain the plate thickness distribution along the width direction of the fin-

ished product outlet. Fig.5 shows the comparison between the measured and calculated plate thickness. It can be seen that the distribution of the two groups is almost the same. In the width direction, the products are often thin on both sides and thick in the middle. The maximum thickness difference of the measured plate thickness of the three groups is 0.17 mm, while that of the calculated plate thickness is 0.14 mm. It can be concluded that the established deformation model of roll system is reliable.

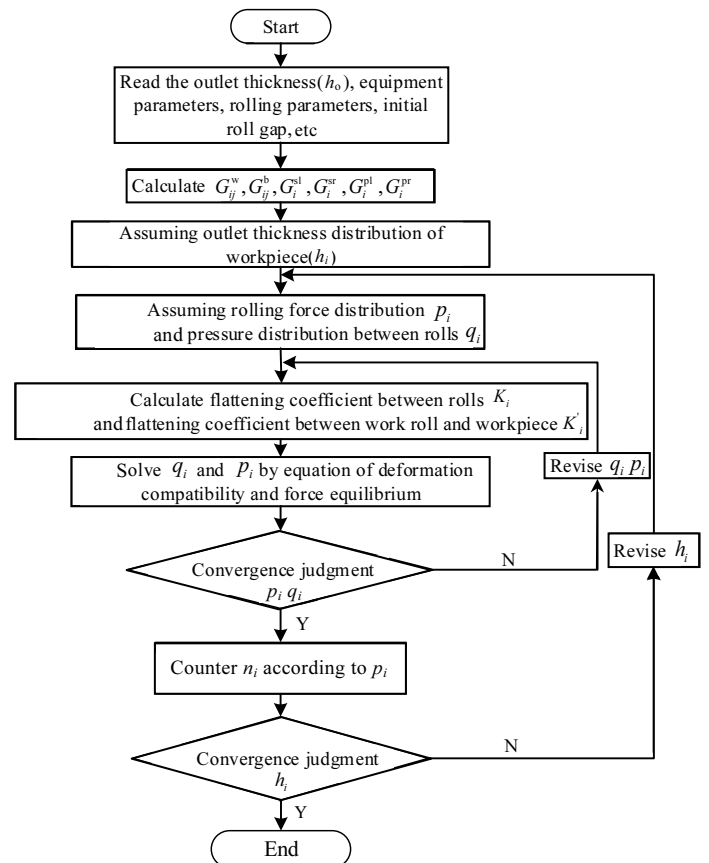


Fig.3 Flow chart of computation

Table 1 Chemical composition of pure titanium billets (wt%)

Fe	O	N	C	H	Ti
0.100	0.120	0.005	0.008	0.001	Bal.

Table 2 Parameters of equipment

Parameters	Value
Work roll diameter/mm	1100
Backup roll diameter/mm	2200
Work roll length/mm	4300
Backup roll length/mm	4600
Equivalent stiffness of mill stand in DS side/kN·mm <sup>-1</sup>	4100
Equivalent stiffness of mill stand in WS side/kN·mm <sup>-1</sup>	4100
Distance of pressure screw/mm	5900
Distance of roll bending cylinder/mm	6040

**Table 3 Basic rolling process parameters**

Pass	Thickness/mm	Rolling reduction/mm	Rolling width/mm	Rolling force/kN	Roll bending force/kN	Average temperature/°C	Rolling speed/m·s <sup>-1</sup>
1	100.54	36.37	1442	14490.3	1095	850	2
2	68.49	31.47	1451	14822.5	1095	816	2.1
3	47.82	20.55	1456	13762.1	1095	798	2
4	30.58	16.95	1460	13959.1	1095	782	2.1
5	27.18	7.59	1461	7960.2	1095	756	2
6	24	3.1	1462	7132.3	1093	705	1.8

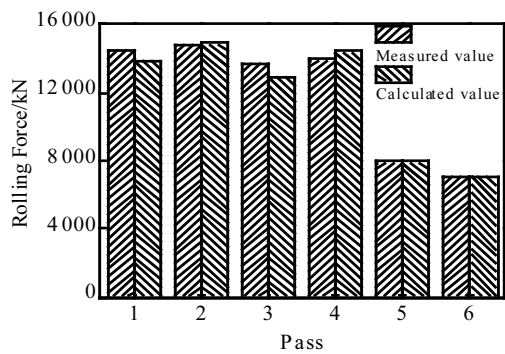


Fig.4 Distribution of rolling forces in each pass

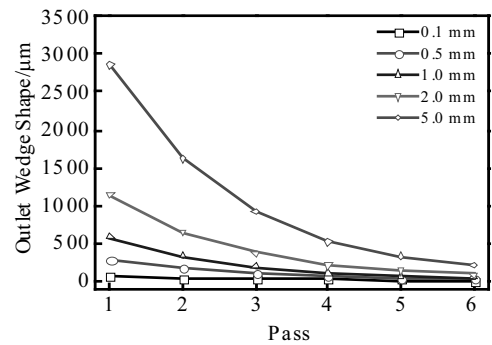


Fig.6 Influence diagram of inlet wedge shape on outlet wedge shape

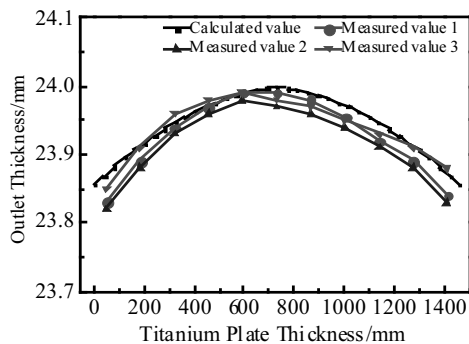


Fig.5 Thickness of the plate along the width

**2.2 Influence of inlet wedge shape of rolling piece on outlet wedge shape**

The rolling blank of pure titanium medium and thick plate is produced by forging blank through mechanical processing. Machining error during the process of mechanical processing will cause the wedge shape of rolling billet section. In order to investigate the influence of inlet wedge shape on outlet wedge shape of the product, the inlet wedge shape of the blank is set as 0.1, 0.5, 1, 2 and 5 mm. The influence of the inlet wedge shape on the outlet wedge shape of the blank during the rolling process is shown in Fig.6. Fig.6 shows that the inlet wedge shape has a significant effect on the outlet wedge shape. The wedge shape change of different passes

shows nonlinear characteristic. With the increase of inlet wedge shape, the outlet wedge shape after six passes of rolling also increases. From the first pass to the sixth pass, the wedge shape produced by the last pass decreases in the next pass of rolling with the gradual accumulation of pass reduction. The sixth pass outlet wedge shape reaches 207 μm at the 5 mm inlet wedge. The sixth pass outlet wedge shape is 41 μm while the inlet wedge shape is 1 mm. At the inlet wedge shape of the rolling piece of 0.5 mm, the sixth pass outlet wedge shape is 21 μm. The sixth pass outlet wedge shape is 4 μm at the 0.1 mm inlet wedge shape. The inlet wedge shape must be less than 0.5 mm, while the product wedge shape needs to be less than 20 μm.

**2.3 Influence of centring error of workpiece on outlet wedge shape**

The geometric center line in the width direction of billet completely coincide with the rolling center line, which is the most ideal rolling state in the rolling process of pure titanium medium and thick plate. However, the actual rolling process is affected by many factors, and the above two lines do not coincide completely, leading to the form of the centring error. In order to investigate the influence of the centring error on the outlet wedge shape of the workpiece, the section of the billet inlet was set as a rectangle with the centring error of 5, 10, 20, 50 and 100 mm, referring to the actual conditions of the industrial site. Fig.7 shows the in-

fluence of blank centring error on outlet wedge. It is observed that the influence of the centring error on the outlet wedge is also obvious, and the wedge shape changes of different passes basically show a linear relationship. The existence of centring error leads to the run off-track on the rolling line of the rolling piece, resulting in a wedge shape caused by the different bouncing on both sides of the frame of each pass. The deviation of the rolling piece and the wedge shape inheritance between passes lead to the aggravation of the wedge shape of subsequent passes. After the centring error reaches 100 mm, the sixth pass outlet wedge shape size is 50  $\mu\text{m}$ ; when the centring error reaches 50 mm, the sixth pass outlet wedge shape size is 25  $\mu\text{m}$ ; the sixth pass outlet wedge shape size is less than 6  $\mu\text{m}$ , while the centring error is less than 20 mm. It can be concluded that the centring error less than 20 mm has little effect on the outlet wedge shape. Therefore, centre position control for the first pass of the rolling billet is very important for reducing the product wedge shape. The centring error should be less than 50 mm, while the product wedge shape should not exceed 20  $\mu\text{m}$ .

#### 2.4 Influence of stiffness difference of mill stand on outlet wedge shape

The overall stiffness of the four-high medium-thickness plate reversing mill is about 8000 kN. The frame stiffness of the left and right sides (transmission side and operation side) may be asymmetric during the manufacturing process of the mill. Generally, the stiffness of the transmission side is greater than that of the operation side. The degree of asymmetry of rigidity in this kind of frame can reach 10%. In order to investigate the influence of the stiffness of mill stand on the outlet wedge shape of the workpiece, the billet inlet section is set as a rectangle, and the stiffness of mill stand on the transmission side is 1%, 5%, 10%, 15% and 20%, higher than that measured by the operation. Fig.8 shows the effect of stiffness difference of mill stand on outlet wedge shape. It is observed that the stiffness difference of mill stand on both sides of the rolling mill has a significant effect on the outlet wedge shape. Different stiffness of mill stand on both sides of the rolling mill leads to different bounces, resulting in wedge shape. Moreover, the wedge

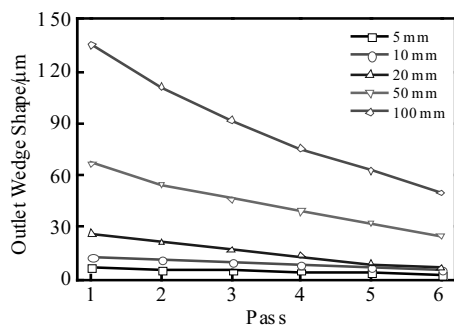


Fig.7 Influence of centring error on wedge size

shape size increases with the increase of the stiffness difference of mill stand on both sides, and the wedge shape changes of different passes show a linear relationship. In order to control the convex degree of the product during practical rolling process, the side rolling reduction of the mill stand with higher rigidity will increase, and the rolling pressure will also increase. Meanwhile, it can partially offset the wedge shape inheritance of the front pass to some extent. When the stiffness difference between the left and right sides of the rolling mill is 20%, the sixth pass outlet wedge shape reaches 45  $\mu\text{m}$ . After the stiffness difference of mill stand reaches 15%, the sixth pass outlet wedge shape size is 32  $\mu\text{m}$ . The sixth pass outlet wedge shape size reaches 23  $\mu\text{m}$ , while the stiffness difference of mill stand is 10%. When the stiffness difference of mill stand is 5%, the sixth pass outlet wedge shape size reaches 15  $\mu\text{m}$ . After the stiffness difference of mill stand reaches 5%, the sixth pass outlet wedge is 5  $\mu\text{m}$ . Therefore, in order to make the wedge shape of the product less than 20  $\mu\text{m}$  and to facilitate the control of plate convex, the stiffness difference of both sides of mill stand should be less than 10%.

#### 2.5 Influence of transverse temperature difference of workpiece on outlet wedge shape

The starting temperature of the pure titanium is about 850  $^{\circ}\text{C}$ . However, the heterogeneity of the temperature inevitably exists due to the heating process of the workpiece in heating furnace or transportation on the roller table. In order to study the influence of transverse (along the width) temperature difference of workpiece on outlet wedge shape, the billet inlet section is set to be rectangular and transverse temperature difference on either side of workpiece is 10, 50, 100, 150 and 200  $^{\circ}\text{C}$ . The transverse temperature distribution is determined by interpolation calculation. Fig.9 shows the influence of transverse temperature difference of workpiece on outlet wedge shape. It is shown that the transverse temperature difference of workpiece has a significant effect on the outlet wedge shape. The main reason is that the transverse temperature difference causes the difference of deformation resistance on both sides of the workpiece, which leads to the difference of deformation

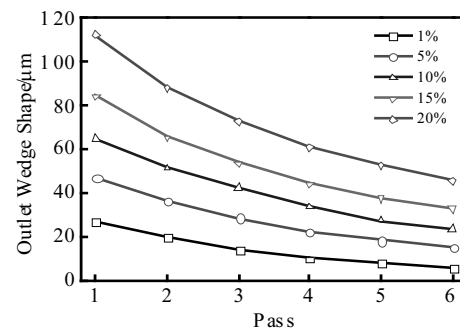


Fig.8 Diagram of influence of the stiffness difference of mill stand on wedge shape

amount of the frame on both side of the rolling mill and the appearance of the outlet wedge shape. The transverse temperature difference tends to decrease with the increase of rolling temperature and the heat conduction of the workpiece. When the transverse temperature difference of workpiece is 200 °C, the sixth pass outlet wedge shape reaches 59 μm, which has an obvious effect on outlet wedge shape. When the transverse temperature difference of workpiece is 150 °C, the sixth pass outlet wedge shape reaches 40 μm. After the transverse temperature difference of workpiece reaches 100 °C, the sixth pass outlet wedge is 21 μm. When the transverse temperature difference of workpiece is 50 °C, the sixth pass outlet wedge reaches 6 μm. When the transverse temperature difference of workpiece is 20 °C, the sixth pass outlet wedge shape reaches 0.2 μm. Therefore, in order to make the wedge shape of this specification product less than 20 μm, workpiece transverse temperature difference should be less than 100 °C.

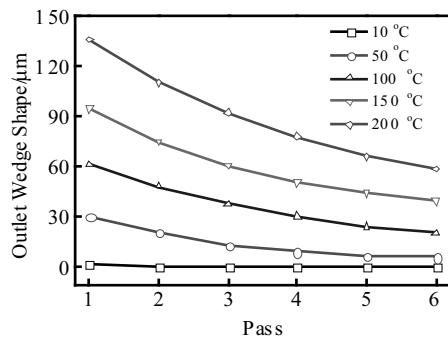


Fig.9 Diagram of influence of transverse temperature difference of workpiece on outlet wedge

### 3 Conclusions

1) The deformation model of double cantilever beam roll system in four-bar rolling mill is established based on the influence function method and coupled asymmetric calculation model, and the reliability of the model is verified. Based on this method, the influence of asymmetric factors on the wedge shape of workpiece section can be investigated.

2) The rolling pressure on both sides of the rolling mill is different due to asymmetrical factors, i.e. inlet wedge shape, centring error, stiffness difference on both sides of the mill stand and transverse temperature difference of the workpiece.

3) The difference of roll system deformation is the basic reason for the wedge shape, and the wedge shape size increases with the increase of deformation difference on both sides of the rolling mill. The centring error and the stiffness difference of the mill stand and the transverse temperature

difference of the workpiece can significantly influence the outlet wedge shape of the workpiece. In terms of single factor's influence on the outlet wedge shape, in order to ensure that the wedge shape of this specification product is less than 20 μm, the inlet wedge shape of workpiece, the centring error, the stiffness difference on both sides of the mill stand and the transverse temperature difference of the workpiece should be less than 0.5 mm, 50 mm, 10% and 100 °C, respectively.

### References

- 1 Fu Y, Xie S S, Xiong B Q et al. *Journal of Wuhan University of Technology: Material Science Edition*[J], 2012, 27(2): 247
- 2 Hardy S J, Biggs D L, Brown K J. *Ironmaking & Steelmaking*[J], 2002, 29(4): 245
- 3 Daun Jeong, Youngil Kang, Yu Jin Jang et al. *ISIJ International*[J], 2013, 53(3): 511
- 4 Gong D Y, Xu J Z, Jiang Z Y et al. *International Journal of Modern Physics B*[J], 2008, 22(31-32): 5734
- 5 Nakhoul R, Montmitonnet P, Legrand N. *International Journal of Material Forming*[J], 2015, 8(2): 283
- 6 Kainz A, Pumhoessel T, Kurz M et al. *International Federation of Automatic Control*[J], 2016, 49-20: 238
- 7 Montague R J, Watton J, Brown K J. *Journal of Materials Processing Technology*[J], 2005, 168(1): 172
- 8 Li Haijun, Xu Jianzhong, Wang Guodong et al. *Journal of Iron and Steel Research International*[J], 2010, 17(3): 21
- 9 Jiang Z Y, Zhu H T, Tieu A K. *Journal of Materials Processing Technology*[J], 2005, 162: 512
- 10 Liu Y, Lee W H. *ISIJ International*[J], 2005, 45(8): 1173
- 11 Liu Jiawei, Zhang Dianhua, Wang Junsheng et al. *Journal of Iron and Steel Research International*[J], 2010, 17(12): 35
- 12 Zhou Hai, Bai Jinlan. *Applied Mechanics and Materials*[J], 2014, 633-634: 791
- 13 Schausberger F, Steinboeck A, Kugi A. *Journal of Process Control*[J], 2016, 47: 150
- 14 Jiang Z Y, Zhu H T, Tieu A K. *International Journal of Mechanical Sciences*[J], 2006, 48(7): 697
- 15 Wang Xiaochen, Yang Quan, Jiang Zhengyi et al. *Steel Research International*[J], 2014, 85(11): 1560
- 16 Mathieu N, Potier-Ferry M, Zahrouni H. *International Journal of Mechanical Sciences*[J], 2017, 122: 267
- 17 Di H S, Xu J Z, Gong D Y et al. *Journal of Material Science and Technology*[J], 2004, 20(3): 330
- 18 Dinh Cuong Tran, Nicolas Tardif, Hamza El Khaloui et al. *Thin-Walled Structures*[J], 2017, 113: 129
- 19 Bai Zhenhua, Han Linfang, Li Jingzhou et al. *Journal of Mechanical Engineering*[J], 2012, 48(20): 77
- 20 Li Jun, Yu Hui, Shi Qingnan et al. *Journal of Central South University*[J], 2016, 47(6): 1888 (in Chinese)

## 非对称因素对热轧纯钛中厚板出口楔形的影响

于 辉<sup>1,2</sup>, 李 伟<sup>1</sup>, 黄兆猛<sup>1</sup>, 王三众<sup>1</sup>, 刘利刚<sup>1</sup>

(1. 燕山大学 机械工程学院, 河北 秦皇岛 066004)

(2. 燕山大学 国家冷轧板带工程技术研究中心, 河北 秦皇岛 066004)

**摘 要:** 针对纯钛中厚板热轧过程中可能出现的轧件断面楔形问题, 结合四辊轧机设备和工艺的非对称特点, 基于影响函数法建立双悬臂梁辊系弹性变形模型, 研究对中误差、机架刚度差、坯料楔形、横向温差等非对称因素对轧件断面楔形的影响。结果表明: 对中误差、机架刚度差、横向温差对出口楔形的影响随着板宽和压下量的增大而增大, 入口楔形对出口楔形的影响随着板宽增大和压下量的减小而增大。

**关键词:** 影响函数法; 纯钛; 热轧; 中厚板; 楔形预测

---

作者简介: 于 辉, 男, 1974 年生, 博士, 教授, 燕山大学机械工程学院, 河北 秦皇岛 066004, E-mail: yuhui@ysu.edu.cn